Available online at www.sciencedirect.com
ScienceDirect
Journal of Sound and Vibration 324 (2009) 556–569
JOURNAL OF SOUND AND VIBRATION
www.elsevier.com/locate/jsvi

Nonlinear flutter of aerothermally buckled composite shells with damping treatments

Won-Ho Shin[a], Il-Kwon Oh[b,*], In Lee[c]

[a]*Factory Automation, Manufacturing Technical Research Center, Samsung Electro-Mechanics, 314, Maetan-Dong, Yeongtong-Gu, Suwon, Gyunggi-Do 443-743, Republic of Korea*
[b]*School of Mechanical Systems Engineering, Chonnam National University, 300 Yongbong-dong, Buk-gu, Gwang-Ju 500-757, Republic of Korea*
[c]*Department of Aerospace Engineering, Korea Advanced Institute of Science and Technology, 373-1 Guseong-Dong, Yuseong-Gu, Daejeon 305-701, Republic of Korea*

Received 29 September 2008; received in revised form 14 February 2009; accepted 21 February 2009
Handling Editor: L.G. Tham
Available online 21 March 2009

Abstract

Finite element analyses of the aerothermoelastic behavior of aerothermally buckled cylindrical composite shells with various damping treatments were implemented using the theory of layerwise displacement field. The arc-length method and iterative nonlinear scheme were taken up to estimate the post-buckling deformation of composite shells due to aerothermal loads. The complex modulus was adopted to take into account the effects of viscoelastic damping. The post-buckling behaviors and aeroelastic characteristics, under thermal loads, of several damped composite shells were investigated with various damping treatments including free layer and constrained layer and sandwiched damping layers. The results show that the flutter boundary of the cylindrical composite panels with viscoelastic layers can be remarkably affected by the aerothermally buckled shapes and damping treatments. Further, the proper damping treatments, coupled with thermal loads, can improve aerothermoelastic characteristics, resulting in the increase of the flutter boundary.

1. Introduction

Generally, the exteriors of vehicles with supersonic speeds become exposed to severe aerodynamic loads as well as environmental temperatures. In a special case, a self-excited oscillation of the external skin can often occur when the velocity increases up to a certain point called the panel flutter speed. Panel flutter is known as a critical, multidisciplinary problem because it is induced by interactions among thermal loads, aerodynamic forces, and elastic restoring forces. Further, it is accompanied with failures or cracks of structures. Adequate understanding of panel flutter is a key prerequisite for the design of high-speed vehicle structures such as launch vehicles, supersonic fighters, and military missiles. Hence, numerous studies of the precise estimation and improvement of the flutter boundary have been undertaken by many researchers. Dowell [1,2] provided a

*Corresponding author. Tel./fax: +82 62 530 1685.
E-mail addresses: wonho78.shin@samsung.com (W.-H. Shin), ikoh@chonnam.ac.kr (I.-K. Oh), inlee@asdl.kaist.ac.kr (I. Lee).

0022-460X/$ - see front matter © 2009 Elsevier Ltd. All rights reserved.
doi:10.1016/j.jsv.2009.02.022

Nomenclature

f_i	body forces
$\mathbf{M}$	mass matrix
$\mathbf{q}$	out-of-balance vector
Q_{ij}	elastic modulus
$\bar{Q}_{ij}$	reduced elastic modulus ($\bar{Q} = R^T Q R$)
ΔT_{cr}	critical buckling temperature
$\mathbf{u}$	unknown displacement DOF vector
u_j, v_j	in-plane displacement at the jth interface
w	transverse displacement
β	aerodynamic pressure parameter
γ	curvature term of Hans Kurmhaar's piston theory
η	loss factor
$\mathbf{\Theta}$	thermal buckling mode
μ	aerodynamic damping parameter
ρ	density of structures
ρ_a	density of airflow
σ_{ij}	Cauchy stress tensor
$\bar{\psi}_k$	shape function

comprehensive review of the mathematical and physical mechanism of panel flutter. Librescu [3] reported pioneering work into the supersonic flutter of shell structures.

Yang and Han [4] developed a simple, finite element method for estimating the panel flutter boundary of a panel that has buckled due to aerodynamic heat. Sawyer [5] obtained the approximate flutter and buckling points of anisotropic laminated plates; he reported that bending-extensional coupling and bending-twisting stiffness destabilizes buckling and flutter characteristics in thin plates. Using Galerkin's method and an arc-length continuation, Chandiramani et al. [6] analyzed the nonlinear dynamic behavior of a buckled composite panel that is subjected to an aerodynamic load which is caused by a high-supersonic flow. By considering nonlinear aerodynamics, they also demonstrated the possibility of hard flutter for such panels. Through a numerical simulation, Wang and Quek [7] found that embedded piezoelectric layers might increase the flutter and buckling capacities of a simply supported beam. Using the finite element method, Lee et al. [8] analyzed thermal post-buckling and aerodynamic-thermal load of cylindrical laminated panels; they suggested that the post-buckling and flutter stabilities might be enhanced by the adoption of shape-memory alloys. Park et al. [9] undertook numerical analyses of composite plates using the first-order shear deformation theory; they showed that the shape-memory alloy could impede the post-buckling deflection. Elfelsoufi and Azrar [10] derived the integral-equation formulation, and investigated the buckling, flutter, and vibration characteristics of beams with variable sections. Seresta et al. [11] conducted parametric studies on the stacking sequences of a flat composite laminate for optimizing the flutter and thermal-buckling behaviors.

Johns and Parks [12] reported that a hysteretic structural damper, which is generally used for dissipating the vibration of a system, destabilized the flutter characteristics of structures. On the contrary, Ellen [13] used spatial derivative arguments to point out that structural damping could stabilize the flutter boundaries of systems. These incompatible results entailed various studies of the relationship between structural damping and flutter characteristics. Oyibo [14] suggested viscous models for both structural and aerodynamic damping, and indicated the dual nature of viscous-damping stabilization or destabilization. Koo and Hwang [15] reported the relationships among structural damping, fiber orientations, and flutter boundary of composite plates. Krause and Dinkler [16] investigated the influence of curvature and damping on flutter behavior. Bismarck-Nasr and Bones [17] studied the damping effects on the panel flutter boundary for thin cylindrical shells. Using a linear finite element approach, Singha and Ganapathi [18] undertook parametric studies of the supersonic flutter behavior of laminated plates in relation to aerodynamic and structural damping as well as thermal loads.

Numerous studies were conducted to improve the flutter boundaries of high-speed vehicles by the use of smart materials. However, the literature survey revealed that the flutter characteristics of shell structures with viscoelastic damping layers had not been investigated considering aerothermally large deformation. This paper first reports an investigation of the nonlinear flutter characteristics, under extreme thermal and aerodynamic conditions, of shell structures with various damping treatments. The layerwise theory was applied in the formulation of the finite element method, and a modified piston supersonic aerodynamic theory [19] was used

to calculate the aerodynamic forces on the surface of the shell structure. Additionally, the complex modulus [20] was adopted to consider the effects of structural damping of the structures.

2. Finite element formulations

2.1. Layerwise displacement field

As shown in Fig. 1, the global in-plane displacement fields (u and v) can be represented in the $r-\varphi-z$ coordinates by the summation of the local in-plane displacement (u_j and v_j) of each laminated interface on the cylindrical coordinate. The transverse deformation of each layer is assumed to be same, so called partial layerwise theory. By introducing the piecewise-linear interpolation function, $\Phi_j(r)$, the layerwise description of the displacements is given as follows:

$$(u,v,w)=\left(\sum_{j=1}^{n_i}u_j(\varphi,z,t)\Phi_j(r),\sum_{j=1}^{n_i}v_j(\varphi,z,t)\Phi_j(r),w(\varphi,z)\right) \tag{1}$$

In Eq. (1), u_i and v_i are, respectively, the axial and hoop displacements at the jth interface, and n_i is the number of laminated layers for each finite element. To save computational time and memory storage through a reduction of n_i, the concept of the sub-lamina of multi-layered structures was applied with a proper thickness-discretization. In previous work [21], the interpolation function and the sub-lamina method has been elucidated well. The interpolation function of $\Phi_j(r)$ with respect to $r-\varphi-z$ coordinate system is the same to $\Phi^J(z)$ with respect to $z-\varphi-x$ coordinate system in Ref. [21]. In the nonlinear strain-displacement relationships, von Kàrmàn's approximation was used for the description of large deformations.

$$\varepsilon_{\varphi\varphi}=\sum_{j=1}^{n_i}\frac{\Phi_j\partial v_j}{r\partial\varphi}+\frac{w}{r}+\frac{1}{2}\left(\frac{\partial w}{r\partial\varphi}\right)^2,\quad \varepsilon_{zz}=\sum_{j=1}^{n_i}\frac{\Phi_j\partial u_j}{\partial z}+\frac{1}{2}\left(\frac{\partial w}{\partial z}\right)^2,\quad \gamma_{r\varphi}=\sum_{j=1}^{n_i}\left\{\frac{v_j\mathrm{d}\Phi_j}{\mathrm{d}r}-\frac{v_j\Phi_j}{r}\right\}-\frac{\partial w}{r\partial\varphi},$$
$$\gamma_{rz}=\sum_{j=1}^{n_i}\frac{u_j\mathrm{d}\Phi_j}{\mathrm{d}r}+\frac{\partial w}{\partial z},\quad \gamma_{\varphi z}=\sum_{j=1}^{n_i}\left(\frac{\partial u_j}{r\partial\varphi}+\frac{\partial v_j}{\partial z}\right)\Phi_j+\left(\frac{\partial w}{\partial z}\right)\left(\frac{\partial w}{r\partial\varphi}\right) \tag{2}$$

2.2. Constitutive and governing equations

For considering the effects of structural damping on the dynamics of the shell structures with viscoelastic layers, the complex modulus, which consists of the stiffness and the loss factor, is adopted. The complex modulus can be expressed in the following form:

$$\bar{E}_{ij}=E_{ij}(1+i\eta_{ij})\quad \text{for } i,j=1,2,3 \tag{3}$$

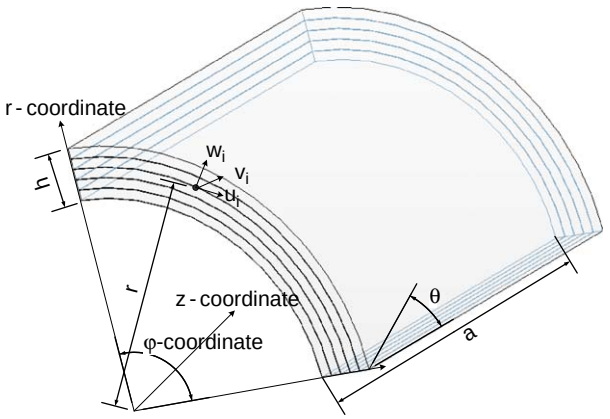

Fig. 1. Global and local coordinates of the cylindrical laminate.

In Eq. (3), the imaginary part of the complex modulus refers to the effect of structural damping. With respect to the material coordinates, the unified linear constitutive equations that relate sinusoidal stresses and strains for the jth lamina of the shell laminates, can be written as

$$\boldsymbol{\sigma}_j = \mathbf{Q}_j \boldsymbol{\varepsilon}_j - \boldsymbol{\alpha}_j \Delta T \tag{4}$$

To consider the ply angle, θ, of the jth lamina of the shell laminate, the modified constitutive equation, with respect to the transformed coordinates, can be written as

$$\boldsymbol{\sigma}_j = \bar{\mathbf{Q}}_j \boldsymbol{\varepsilon}_j - \bar{\boldsymbol{\alpha}}_j \Delta T \tag{5}$$

Through the assumption of zero transverse normal stress, the reduced constitutive equation can be represented as follows:

$$\tilde{\boldsymbol{\sigma}}_j = \tilde{\mathbf{Q}}_j \tilde{\boldsymbol{\varepsilon}}_j - \tilde{\boldsymbol{\alpha}}_j \Delta T \tag{6}$$

In Eq. (6), the subscript j indicates the layer-number, and $\tilde{\mathbf{Q}}_j$ and $\tilde{\boldsymbol{\alpha}}_j$ are, respectively, the reduced complex stiffness matrix (5×5) and the coefficients of the thermal-expansion vector (5×1). The detailed terms of the stiffness matrix and thermal-expansion vector were well-described in earlier studies [22,23].

Hamilton's principle can be applied to derive the governing equations for the damped composite shells in which viscoelastic material is embedded.

$$\int_V (\rho \ddot{u}_i \delta u_i + \sigma_{ij} \delta \varepsilon_{ij} - f_i \delta u_i)\, \mathrm{d}V = \int_S \tau_i \delta u_i \, \mathrm{d}S \tag{7}$$

By adopting Hamilton's formulations and layerwise displacement fields, the nonlinear, finite element equation for damped composite shells can be obtained in the following form:

$$\mathbf{M}_e \ddot{\mathbf{u}}_e + (\mathbf{K}_e - \mathbf{K}_e^{\Delta T} + \mathbf{L}_e)\mathbf{u}_e = \mathbf{F}_e^{\Delta T} + \mathbf{F}_e^{aerodynamic} \tag{8}$$

In Eq. (8), $\mathbf{M}_e$, $\mathbf{K}_e$, $\mathbf{K}_e^{\Delta T}$, $\mathbf{L}_e$, $\mathbf{F}_e^{\Delta T}$, and $\mathbf{F}_e^{aerodynamic}$ are, respectively, the mass matrix, the linear complex stiffness matrix, the thermal geometric stiffness matrix, the nonlinear stiffness matrix, the thermal loading vector, and the external force vector. The detailed derivations of $\mathbf{L}_e$ were elucidated in prior literature [21]. Through an assembly procedure, the global finite element equation of composite shells that are subject to a thermal load and an aerodynamic force can be obtained.

$$\mathbf{M}\ddot{\mathbf{u}} + (\mathbf{K} - \lambda_T \mathbf{K}^{\Delta T} + \mathbf{L}(\mathbf{u}))\mathbf{u} = \lambda_T \mathbf{F}^{\Delta T} + \mathbf{F}^{aerodynamic} \tag{9}$$

In Eq. (9), $\mathbf{K}^{\Delta T}$, $\mathbf{F}^{\Delta T}$, λ_T, and $\mathbf{F}^{aerodynamic}$ are, respectively, the global thermal geometric complex stiffness, the global thermal loading vector under a unit-load level of temperature increment, the load level, and the global aerodynamic force vector. The aerodynamic forces can be calculated by the modified piston theory [19]. By substituting for these forces in Eq. (9), the final aerothermoelastic equations are obtained as given below:

$$\mathbf{M}\ddot{\mathbf{u}} + \mu \mathbf{A}_\mu \dot{\mathbf{u}} + (\mathbf{K} - \lambda_T \mathbf{K}^{\Delta T} + \mathbf{L}(\mathbf{u}) + \beta \mathbf{A}_\beta - \gamma \mathbf{A}_\gamma)\mathbf{u} = \lambda_T \mathbf{F}^{\Delta T} \tag{10}$$

In Eq. (10), β, μ, and γ are the aerodynamic pressure parameter, the damping parameter, and the radius coefficient, respectively. Prior to an analysis of the post-buckling behavior, the reference rise in the buckling temperature is determined by Euler buckling analysis.

$$(\mathrm{Re}[\mathbf{K}] - \Delta T_{cr} \mathbf{K}^{\Delta T})\boldsymbol{\Theta} = \mathbf{0} \tag{11}$$

In Eq. (11), ΔT_{cr} and $\boldsymbol{\Theta}$ are the critical buckling temperature and the buckling mode. The buckled mode shapes are properly scaled to an initial deflection for the nonlinear stiffness matrix at the post-buckling range.

Provided that the post-buckled structure experiences a small vibration that follows a large buckled deflection, the aerothermoelastic solution can be represented as the summation of the time-invariant solution with large deflection, $\mathbf{u}_s$, and the time-variant solution with small amplitude, $\mathbf{u}_t$. By substituting this summation in Eq. (10), the static and dynamic coupled equations can be obtained as follows:

$$\mathbf{q}(\mathbf{u}_s, \lambda_T) = (\mathrm{Re}[\mathbf{K}] - \lambda_T \mathbf{K}^{\Delta T} + \mathrm{Re}[\mathbf{L}(\mathbf{u}_s)] + \beta \mathbf{A}_\beta - \gamma \mathbf{A}_\gamma)\mathbf{u}_s - \lambda_T \mathbf{F}^{\Delta T} = 0 \tag{12}$$

$$\mathbf{M}\ddot{\mathbf{u}}_t + \mu \mathbf{A}_\mu \dot{\mathbf{u}}_t + (\mathbf{K} - \lambda_T \mathbf{K}^{\Delta T} + \mathbf{L}(\mathbf{u}_s) + \beta \mathbf{A}_\beta - \gamma \mathbf{A}_\gamma)\mathbf{u}_t = \mathbf{0} \tag{13}$$

In Eq. (12), $\mathbf{q}(\mathbf{u}_s, \lambda_T)$ is the out-of-balance vector. From Eq. (12), the post-buckled deflection, $\mathbf{u}_s$, arising from a thermal load, an aerodynamic force, and a restoring force, is calculated using arc-length iterative methods. Additionally, only the real parts of the complex stiffness matrix are used to estimate the static thermo-aerodynamic buckled deflection given that the structural damping terms take effect only for dynamic problems. By substituting the calculated $\mathbf{u}_s$ into Eq. (13), the aerothermoelastic solution can be obtained as the complex eigenvalues, Λ_β. The solution varies with the increment of the aerodynamic pressure, and the critical aerodynamic pressure is β when the imaginary parts of the solutions change from being negative to being positive. The modal frequencies and loss factors at β are defined as the real and imaginary parts, respectively, of the complex solution of Eq. (13).

$$\omega_\beta^2 = \mathrm{Re}[\Lambda_\beta], \quad \eta_\beta = \mathrm{Im}[\Lambda_\beta]/\mathrm{Re}[\Lambda_\beta] \tag{14}$$

3. Results and discussion

3.1. Post-buckling analysis of composite shells with viscoelastic layers

The variation, with thermal load, of the post-buckling behavior of the cylindrical composite shells with viscoelastic layers, consisting of 14 graphite/epoxy layers and a viscoelastic layer as shown in Fig. 2, was investigated. The properties of the materials used for the analyses were as follows.

Graphite/epoxy:

$$\rho_g = 1570\,\mathrm{kg/m^3}, \quad E_{g1} = 119\,\mathrm{Gpa}, \quad E_{g2} = 8.67\,\mathrm{Gpa}, \quad G_{g12} = G_{g13} = 5.18\,\mathrm{Gpa}, \quad G_{g23} = 3.9\,\mathrm{Gpa}$$
$$v_{g12} = 0.31, \quad \eta_{g1} = 1.18 \times 10^{-3}, \quad \eta_{g2} = 6.20 \times 10^{-3}, \quad \eta_{g12} = \eta_{g13} = 8.12 \times 10^{-3}, \quad \eta_{g23} = 8.46 \times 10^{-3}$$

Viscoelastic layer (ISD 112-3M):

$$\rho_d = 986.8\,\mathrm{kg/m^3}, \quad E_d = 11.2\,\mathrm{Mpa}, \quad G_d = 3.76\,\mathrm{Mpa}, \quad v_d = 0.49, \quad \eta_d = 1.02$$

In the finite element models, 8×8 meshes with nine-node elements were adopted for the in-plane direction, as were five sub-laminates in the thickness direction. Further, all the edges of the cylindrical shell were clamped. Prior research has described in detail the validation of this method and the convergence test of mesh size [22].

Fig. 3 displays the thermal-deformation behavior at the central position of the panels expressed in terms of the variation of thermal environments. The thermally deformed configuration of the undamped composite shell with the $[0_4/90_3]_s$ laminate resembles a plateau, and its central displacement rises smoothly with the thermal load. In terms of the thermal-deformation behavior, the damped composite shells can be divided into two groups: A and B. Group A includes the $[D/0_4/90_3/90_3/0_4]$ and $[0_4/90_3/90_3/0_4/D]$ laminates, which also have plateau-shaped geometries. Generally, those laminate sequences are called free layer damping models. Additionally, the changes of their central deformations with incremental thermal load are similar to that of the

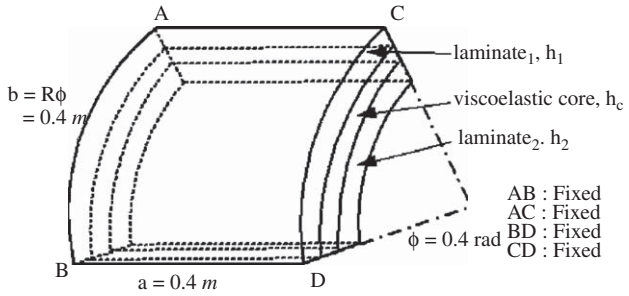

Fig. 2. Geometry and construction of the composite shell with a viscoelastic layer.

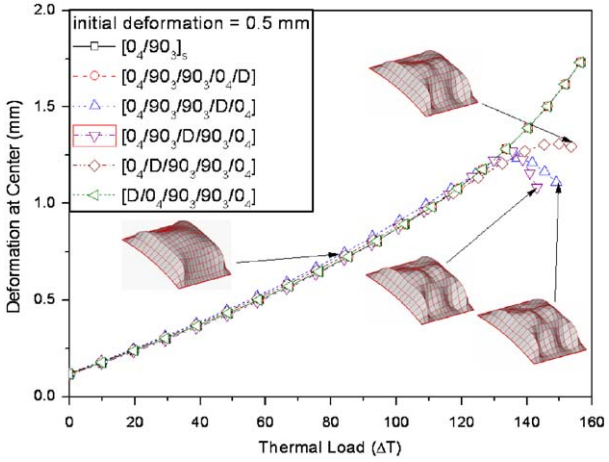

Fig. 3. Thermal post-buckling behavior of composite shells with various damping treatments.

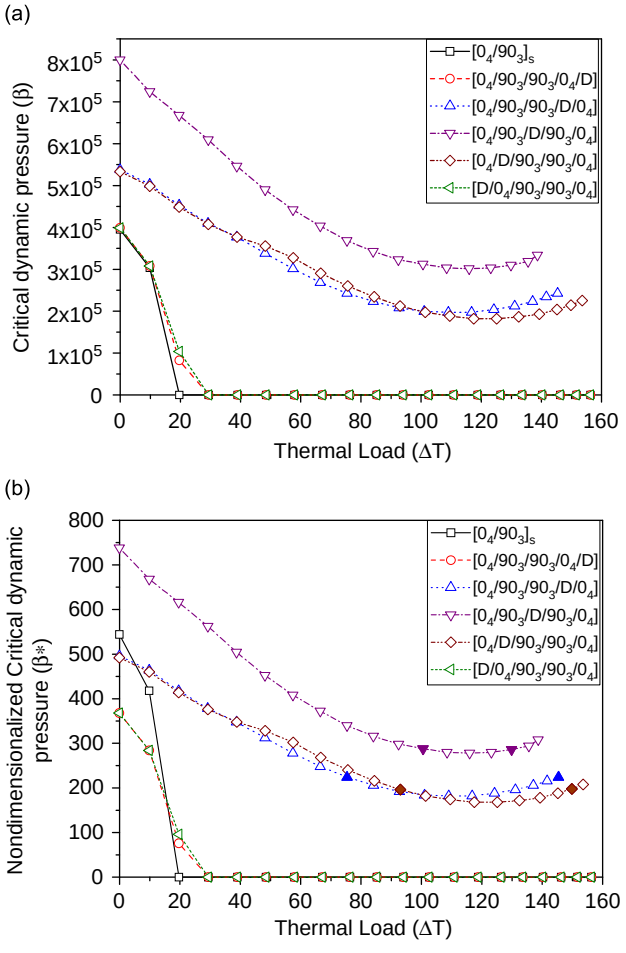

Fig. 4. Variation of the flutter boundaries of various composite shells with thermal loads: (a) flutter boundary, (b) nondimensionalized flutter boundary.

undamped composite shell. Group B contains the $[0_4/D/90_3/90_3/0_4]$, $[0_4/90_3/D/90_3/0_4]$, and $[0_4/90_3/90_3/D/0_4]$ laminates; Group B is classified into constrained layer damping models. Further, it manifests similar thermal deformation to Group A, up to the vicinity of $\Delta T = 130$. However, beyond $\Delta T = 130$, dramatic changes occur to the thermally deformed shapes. In particular, the thermal deformation of Group B has two humps, and the central deformation of the group decreases with the incremental thermal load because of the change in the deformed shape. Moreover, the closer the viscoelastic layer is embedded to the neutral axis of the shell, the sharper is the decrease in the central deformation. Since the damping factor cannot affect the static deformations of shells, this trend may result from the increased in-plane flexibility that is induced by the relatively low stiffness of the embedded viscoelastic layer.

These results confirm that the in-plane stiffness of the structure can considerably affect its thermal-deformation behavior. Further, the damping treatments for dynamic stability of the structures may induce unexpected changes in the thermal characteristics.

3.2. Aerothermoelastic characteristics of damped composite shells

Aerothermoelastic analyses were conducted for the finite element model adopted in the previous section. Fig. 4(a) indicates the variation, with thermal load, of the critical dynamic pressure of various damped composite shells. Without the thermal load, the panel flutter of the undamped composite shell occurs at

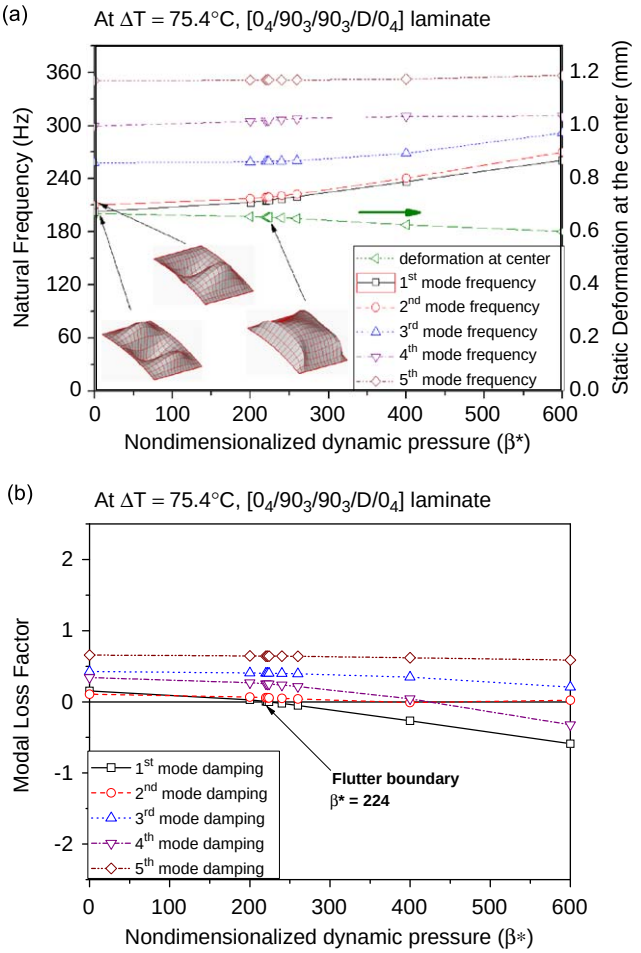

Fig. 5. Flutter history of the $[0_4/90_3/90_3/D/0_4]$ laminate at $\Delta T = 75.4\,^{\circ}C$: (a) Natural frequencies and aerothermoelastic deformation at the center and (b) Modal loss factors.

$\beta = 3.95 \times 10^5$. For this shell, the critical dynamic pressure steeply decreases to zero with the augmentation of the thermal load, and remains zero above $\Delta T = 19.7$, which means the structure is aeroelastically quite unstable. The flutter boundaries of Group A improve a little in comparison with that of the undamped shell. There are a few differences between the $[D/0_4/90_3/90_3/0_4]$ and $[0_4/90_3/90_3/0_4/D]$ laminates, but the variations of their respective flutter boundaries are almost similar to each other. Without the thermal load, the flutter of Group A occurs at $\beta = 3.99 \times 10^5$, which is one percent higher than that for the undamped composite shell. Additionally, the critical dynamic pressure drops to zero above $\Delta T = 29.4$, which suggests that Group A is rather aerothermoelastically stable in comparison with the undamped composite shell.

In contrast with the two preceding cases, the critical dynamic pressure of Group B decreases with rising thermal load up to a certain value, but increases with additional thermal load. This behavior may be induced by the changes of the thermally buckled shapes, whereby two different flutter modes can exist at the same dynamic pressure in certain regimes. The variations of the flutter boundaries of the $[0_4/D/90_3/90_3/0_4]$ and $[0_4/90_3/90_3/D/0_4]$ laminates are similar to each other up to the vicinity of $\Delta T = 40$, but the differences between the two cases become conspicuous above that point. Without the thermal load, their flutters occur at $\beta = 5.37 \times 10^5$ and 5.33×10^5, respectively. The results shown in the figures indicate that the flutter values are about 36 percent greater than that of the undamped composite shell. Additionally, the critical dynamic pressure of the $[0_4/D/90_3/90_3/0_4]$ laminate starts to rise above $\Delta T = 105.0$; in contrast, that of

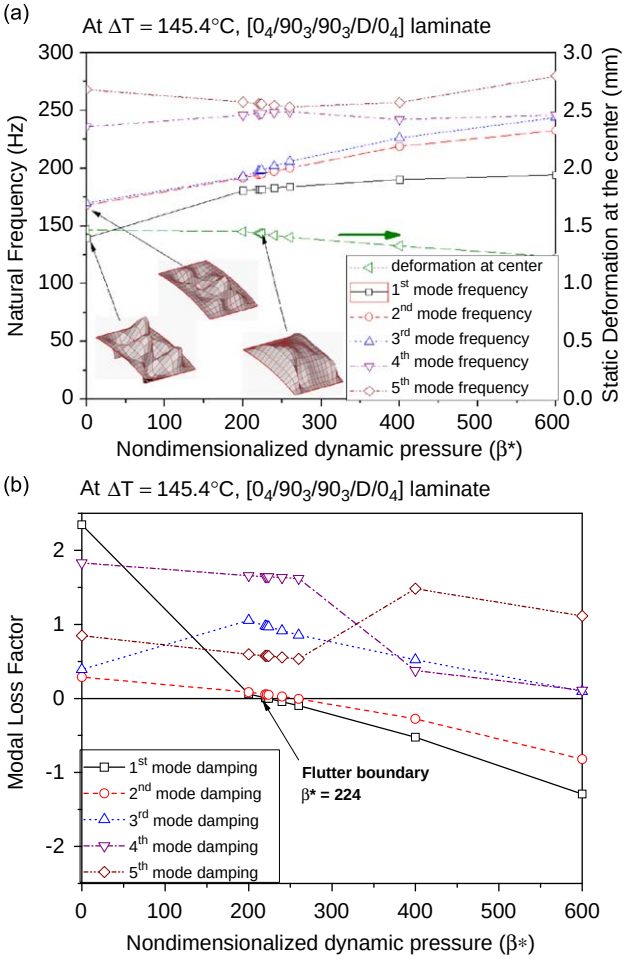

Fig. 6. Flutter history of the $[0_4/90_3/90_3/D/0_4]$ laminate at $\Delta T = 145.4\,^{\circ}C$: (a) Natural frequencies and aerothermoelastic deformation at the center and (b) modal loss factors.

$[0_4/90_3/90_3/D/0_4]$ starts to rise only above $\Delta T = 128.8$. In the absence of thermal loads, the flutter of the $[0_4/90_3/D/90_3/0_4]$ laminate occurs at $\beta = 8.00 \times 10^5$. Further, of all the shells, this laminate has the largest critical pressure, resulting in a 102 percent improvement over the undamped composite shell.

These results reveal that damping treatments appreciably improve the flutter boundaries, and that the nearer the damping layers are buried to the central line of the thickness direction, the stronger are the aerothermoelastic stabilities. However, due to the differing thicknesses, a direct comparison between undamped and damped composite shells is rather unfair and misleading. More specifically, damped composite shells are thicker than undamped shells on account of the embedded viscoelastic layer. Therefore, nondimensionalization of the critical dynamic pressure is necessary for reasonable comparison between undamped and damped composite shells. Fig. 4(b) presents the nondimensionalized flutter boundaries of the various composite shells with reference to the augmentation of the thermal loads. In the absence of thermal loads, the nondimensionalized, critical dynamic pressures (β^*) of the damped composite shells are lower than that of the undamped shell, except for the $[0_4/90_3/D/90_3/0_4]$ laminate. However, the flutter boundary of the undamped composite shell drops steeply as the thermal load increases, and the β^*s of all the damped composite shells are greater than that of the undamped shell above $\Delta T = 20.0$. It is difficult to definitively confirm that damping treatments improve the aeroelastic stabilities of general shell structures. However, from previous results, it can be conservatively asserted that the embedded viscoelastic layers might reduce the falls in the flutter boundaries that are induced by thermal loads.

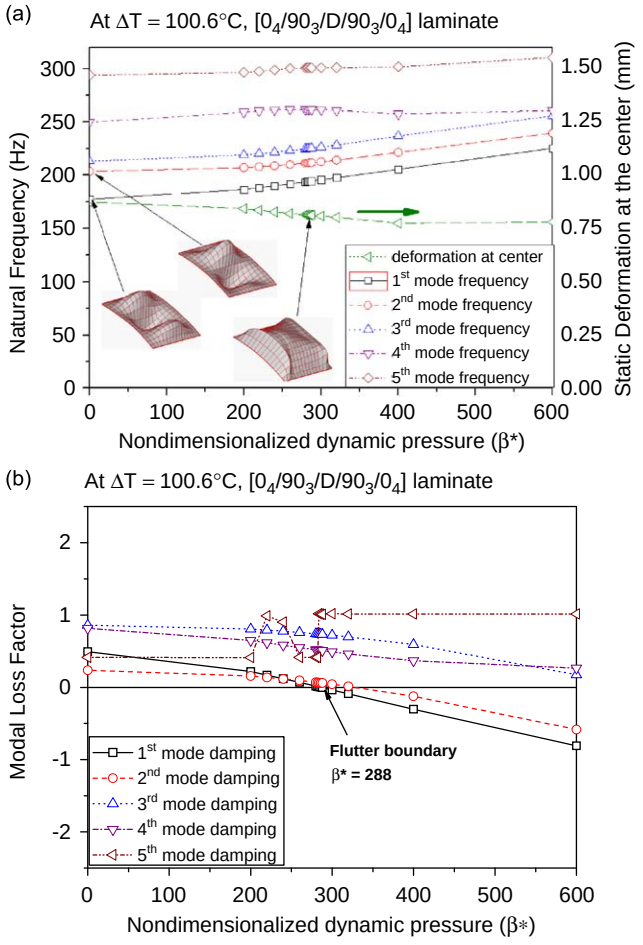

Fig. 7. Flutter history of the $[0_4/90_3/D/90_3/0_4]$ laminate at $\Delta T = 100.6\,^{\circ}C$: (a) Natural frequencies and aerothermoelastic deformation at the center and (b) modal loss factors.

To investigate in more detail the upswings in the flutter boundaries of group B following changes in the thermally deformed shapes, the histories of the two different flutters that correspond to the same β^* were examined for the solid marks (▲, ▼, ♦) indicated in Fig. 4(b). Figs. 5 and 6 depict the flutter histories of the $[0_4/D/90_3/90_3/0_4]$ laminate with respect to increments of β^* both before and after the change of the deformed shape (▲). Fig. 5(a) indicates the five lowest natural frequencies and the central aerothermal deformations of the shell laminate at $\Delta T = 75.4$. All the natural frequencies lie in the range [200, 360 Hz], and smoothly increase with β^*. Their mode shapes are observed as C3L1, C2L1, C3L2, C4L2, and C3L3, respectively, where Cn and Lm refer to the numbers of circumferential and longitudinal waves, respectively. A plateau-shaped deformation that arises from the aero-thermal loads is also observed. The deflection of the central point decreases slowly with increments of β^*. Fig. 5(b) reveals the five lowest modal loss factors, which are all smaller than 1, and decrease with increasing β^*. The loss factor of the first mode becomes negative at $\beta^* = 224$ as the first and second modes are coalescent; this implies the occurrence of the panel flutter. Fig. 6(a) also shows the natural frequencies and the central deformations at $\Delta T = 145.4$. The natural frequencies lie in the range [140, 280 Hz] and, except for the fifth mode, steadily increase with increments of β^*. The mode shapes are C3L4, C4L3, C3L3, C4L4, and C3L5, respectively. Complex mode changes among the five lowest modes are observed in the vicinity of the flutter boundary. A deformation with two humps is induced by the aerothermal load, and its magnitude is almost twice as big as that in Fig. 5(a) because of the difference in the thermal loads. Further, the peak heights of the two humps smoothly reduce with increasing β^*. Fig. 6(b)

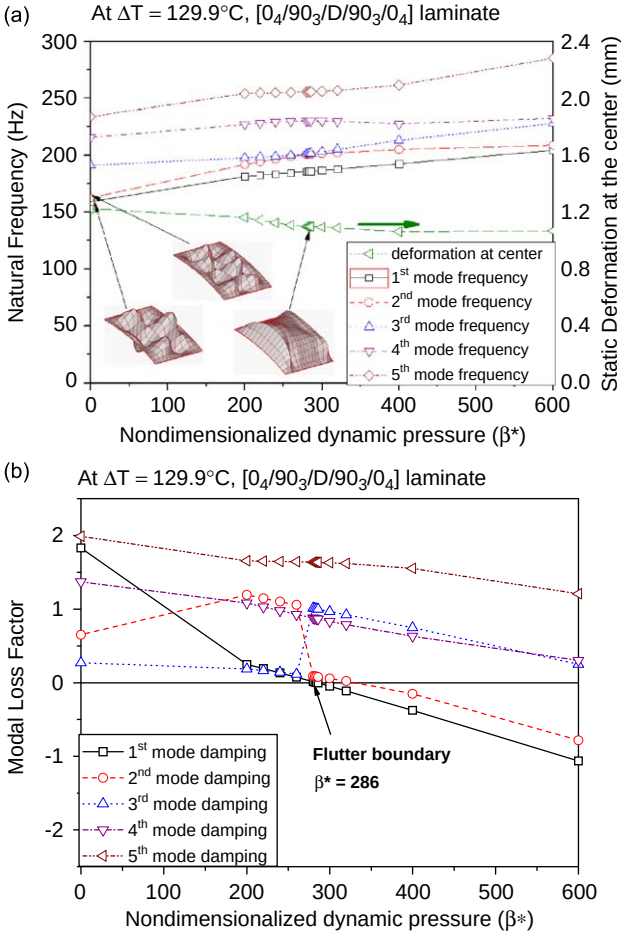

Fig. 8. Flutter history of the $[0_4/90_3/D/90_3/0_4]$ laminate at $\Delta T = 129.9\,^{\circ}C$: (a) Natural frequencies and aerothermoelastic deformation at the center and (b) modal loss factors.

indicates the five lowest modal loss factors, which are larger than those of Fig. 5(b). The loss factor of the first mode becomes negative at $\beta^* = 224$ because of the coalescence between the first and second modes, and stays negative until the critical dynamic pressure for $\Delta T = 95.4$. These results clarify that in contrast to the modal frequencies, the modal loss factors for $\Delta T = 145.4$ are higher than those for $\Delta T = 95.4$. The improvement in the modal loss factors seems to cause the flutter boundaries to upswing after the change of the thermally deformed shape in Fig. 4. The increments of the modal loss factors result from the sudden increment of $\mathbf{K}^{\Delta T}$, due to the altered geometry of the deformed shape. As presented in Eq. (14), the modal loss factors are defined as the ratios between the real and imaginary parts of the complex eigenvalues. The geometric nonlinear stiffness, $\mathbf{L}$, increases both the real and imaginary terms, and $\mathbf{K}^{\Delta T}$ reduces only the real parts of Eq. (13) with increasing ΔT. Consequently, the modal frequencies drop due to the decrease of the real parts of the complex eigenvalues, and the modal loss factors increase in as much as the imaginary parts increase and the real parts decrease.

Figs. 7 and 8 indicate the flutter histories of the $[0_4/90_3/D/90_3/0_4]$ laminate with respect to increments of β^* both below and above the inflection of the flutter boundaries (▼). Fig. 7(a) denotes the five lowest natural frequencies and the central aerothermal deformations of the shell laminate at $\Delta T = 100.6$. All the natural frequencies lie in the range, [170, 300 Hz], and steadily increase with β^*. In addition, their mode shapes are obtained as C3L1, C4L1, C3L2, C4L2, and C4L3, respectively. A plateau-shaped deformation induced by the aero-thermal loads is obtained, and its deflection at the central point decreases slowly with increasing β^*. Fig. 7(b) shows the five lowest modal loss factors with magnitudes smaller than 1; these factors reduce with

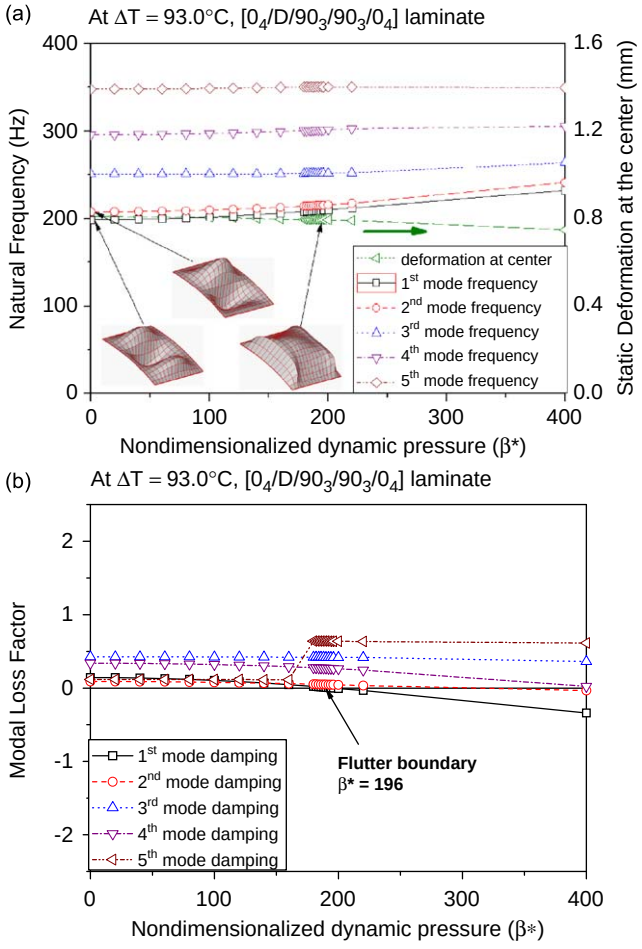

Fig. 9. Flutter history of the $[0_4/D/90_3/90_3/0_4]$ laminate at $\Delta T = 93.0\,^{\circ}C$: (a) Natural frequencies and aerothermoelastic deformation at the center and (b) modal loss factors.

increments of β^*. The loss factor of the first mode becomes negative at $\beta^* = 288$, and determines the flutter boundary. Fig. 8(a) presents the natural frequencies and central deformations at $\Delta T = 129.9$. The natural frequencies lie between 150 and 280 Hz. They increase smoothly with β^*, and the mode shapes are observed as C3L2, C4L3, C3L3, C3L2′, and C4L2, respectively. The first and fourth modes have the same modal wavenumber, but differ with respect to the phase. A thermally deformed shape similar to the one at $\Delta T = 100.6$ is observed, implying that the changes of the deformed shape have not yet occurred. Fig. 8(b) denotes the five lowest modal loss factors with higher magnitudes compared with those of Fig. 7(b). The loss factor of the first mode is negative at $\beta^* = 286$, similar to the flutter boundary for $\Delta T = 100.6$. Though the deformed shapes are not altered, an upswing of the flutter boundaries is observed. These results indicate that with increasing thermal loads, the flutter boundaries rapidly decrease at first because of the increment of $\mathbf{K}^{\Delta T}$. Subsequently, the curve of the flutter boundary flattens before rising because of the increasing nonlinear stiffness, $\mathbf{L}$. Finally, the increment of flutter boundaries is accelerated given the changes of the thermally deformed shape.

Figs. 9 and 10 show the flutter histories of the $[0_4/90_3/90_3/D/0_4]$ laminate against increments of β^* both before and after the change of the deformed shape (♦). Fig. 9(a) presents the five lowest natural frequencies with mode shapes as C3L1, C2L1, C3L2, C4L2, and C3L3, and the plateau-shaped, central aerothermal deformations at $\Delta T = 93.0$. Fig. 9(b) indicates the five lowest modal loss factors, and the flutter occurs at $\beta^* = 196$ in the first mode. Fig. 10(a) also depicts the five lowest natural frequencies with mode shapes as C3L2, C3L2′, C2L1, C3L3, and C4L2, and the central aerothermal deformations with a two-humped shape at

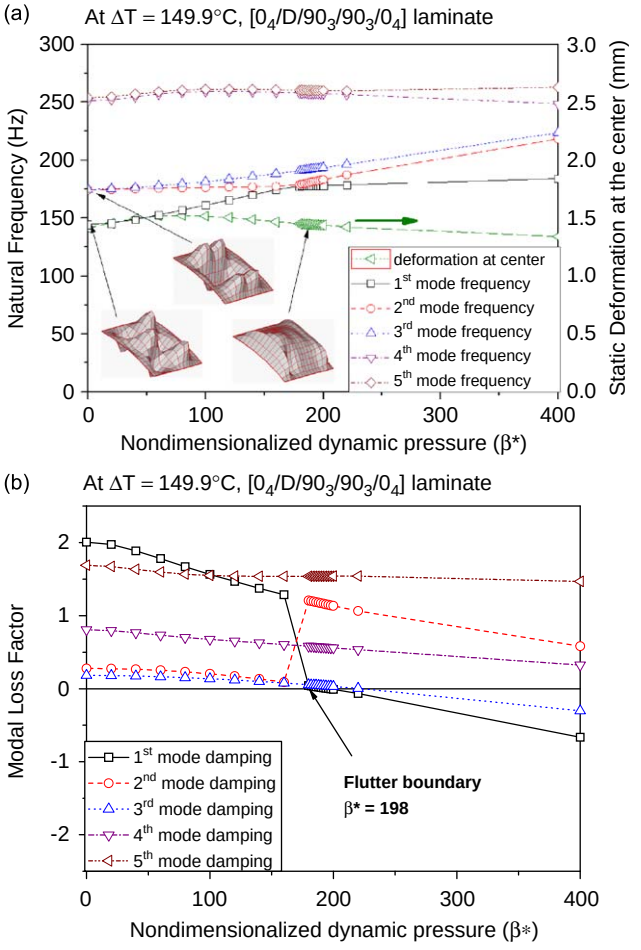

Fig. 10. Flutter history of the $[0_4/D/90_3/90_3/0_4]$ laminate at $\Delta T = 149.9\,^{\circ}C$: (a) Natural frequencies and aerothermoelastic deformation at the center and (b) modal loss factors.

$\Delta T = 149.9$. Fig. 10(b) presents the five lowest modal loss factors, and the flutter occurs at $\beta^* = 198$ in the first mode. The behaviors of the aerodynamic and thermal-deformation characteristics with increasing β^* are similar to those of the $[0_4/D/90_3/90_3/0_4]$ laminate.

4. Conclusion

Using the layerwise finite element method, aerothermoelastic static and dynamic stabilities of cylindrical composite shells with embedded viscoelastic layers were investigated in this study. The aerothermally nonlinear deformations and aerothermoelastic flutter boundaries of various damped composite shells with different damping treatments such as free, constrained and sandwiched viscoelastic layers were investigated by varying the thermal loading. Present results clarify that the laminate sequences with viscoelastic and constrained layers may remarkably affect the aerothermally deformed shape, and that the deformed shapes can influence the flutter boundaries of damped composite shells. Additionally, the results reveal that the nonlinear stiffness that is induced by transverse large deformations can improve the aerothermoelastic characteristics of the damped composite shells above the high temperature region. Further, the proper damping treatments, which are highly coupled with aerothermal loads, can improve aerothermoelastic characteristics, resulting in the increase of the flutter boundary of the cylindrical composite panels.

Acknowledgments

This work was supported by the Korea Science and Engineering Foundation (KOSEF) NRL Program Grant funded by the Korea government (MEST) (No. R0A-2008-000-20012-0).

References

[1] E.H. Dowell, Panel flutter: a review of the aeroelastic stability of plates and shells, *AIAA Journal* 8 (1970) 385–399.
[2] E.H. Dowell, Flutter of a buckled plate as an example of chaotic motion of a deterministic autonomous system, *Journal of Sound and Vibration* 85 (1982) 333–344.
[3] L. Librescu, *Elastostatics and Kinetics of Anisotropic and Heterogeneous Shell-Type Structures*, Noordhoff International Publishing, Leyden, The Netherlands, 1975.
[4] T.Y. Yang, A.D. Han, Flutter of thermally buckled finite element panels, *AIAA Journal* 14 (1976) 975–977.
[5] J.W. Sawyer, Flutter and buckling of general laminated plates, *Journal of Aircraft* 14 (1977) 387–393.
[6] N.K. Chandiramani, R.H. Plaut, L.I. Librescu, Non-linear flutter of a buckled shear deformable composite panel in a high-supersonic flow, *International Journal of Non-Linear Mechanics* 30 (1995) 149–167.
[7] Q. Wang, S.T. Quek, Enhancing flutter and buckling capacity of column by piezoelectric layers, *International Journal of Solids and Structures* 39 (2002) 4167–4180.
[8] I. Lee, J.H. Roh, I.K. Oh, Aerothermoelastic phenomena of aerospace and composite structures, *Journal of Thermal Stresses* 26 (2003) 525–546.
[9] J.S. Park, J.H. Kim, S.H. Moon, Thermal post-buckling and flutter characteristics of composite plates embedded with shape memory ally fibers, *Composites: Part B* 36 (2005) 627–636.
[10] Z. Elfelsoufi, L. Azrar, Buckling, flutter and vibration analyses of beams by integral equation formulation, *Computers and Structures* 83 (2005) 2632–2649.
[11] O. Seresta, M.M. Abdalla, S.B. Mulani, P. Marzocca, Stacking sequence design of flat composite panel for flutter and thermal buckling, *AIAA Journal* 44 (2006) 2726–2764.
[12] D.J. Johns, P.C. Parks, Effect of structural damping on panel flutter, *Aircraft Engineering* 32 (1960) 304–308.
[13] C.H. Ellen, Influence of structural damping on panel flutter, *AIAA Journal* 6 (1968) 2169–2174.
[14] G.A. Oyibo, Unified panel flutter theory with viscous damping effects, *AIAA Journal* 21 (1983) 767–773.
[15] K.N. Koo, W.S. Hwang, Effects of hysteretic and aerodynamic damping on supersonic panel flutter of composite plates, *Journal of Sound and Vibration* 273 (2004) 569–583.
[16] H. Krause, D. Dinkler, The influence of curvature on supersonic panel flutter, *Proceedings of the 39th AIAA/ASME/ASCE/AHS/ASC Structures, Structural Dynamics, and Material Conference AIAA-98-1841*, 1998, pp. 1234–1240.
[17] M.N. Bismarck-Nasr, C.A. Bones, Damping effects in nonlinear panel flutter, *AIAA Journal* 38 (2000) 711–713.
[18] M.K. Singha, M. Ganapathi, A parametric study on supersonic flutter behavior of laminated composite skew flat panels, *Composite Structures* 69 (2005) 55–63.
[19] H. Krumhaar, The accuracy of linear piston theory when applied to cylindrical shells, *AIAA Journal* 1 (1963) 1448–1449.
[20] M. L. Drake, Damping properties of various materials, Technical Report AFWAL-TR-88-4248, 1989.

[21] I.K. Oh, I. Lee, Thermal snapping and vibration characteristics of cylindrical composite panels using layerwise theory, *Composite Structures* 51 (2001) 49–61.
[22] I. Lee, I.K. Oh, W.H. Shin, K.D. Cho, K.N. Koo, Dynamic characteristics of cylindrical composite panels with co-cured and constrained viscoelastic layers, *JSME International Journal, Series C* 45 (2000) 16–25.
[23] W.H. Shin, I.K. Oh, J.H. Han, I. Lee, Aeroelastic characteristics of cylindrical hybrid composite panels with viscoelastic damping treatments, *Journal of Sound and Vibration* 296 (2006) 99–116.